Jurnal Teknologi Kedirgantaraan (JTK)
Vol. 10, No. 2, August 2025, page. 222-231
ISSN: 2528-2778 (Print); 2684-9704 (Online)
https://doi.org/10.35894/jtk.v10i2.128

JTK
Jurnal Teknologi Kedirgantaraan
(Journal of Aeronautical Engineering)

Numerical Study on the Comparative Structural Behavior of Auxetic Chiral and Honeycomb Structures Under Compression and Impact Loading

Simon Sindhu Hendradjaja, Febri Algazali, Syarifah Fairuza, Budi Aji Warsiyanto*, Riskha Agustianingsih

Study Program of Aeronautical Engineering, Faculty of Aerospace and Industrial Engineering, Universitas Dirgantara Marsekal Suryadarma, Indonesia

Article Info

Article History:
Submitted: September 8th, 2024
Revised: July 30th, 2025
Accepted: August 26th, 2025

Keywords:
auxetic, honeycomb, impact loading, numerical simulation, and sandwich structure.

ABSTRACT

This study aims to compare the structural performance of auxetic chiral and honeycomb sandwich panels under compression and impact loading to identify their potential application in lightweight aerospace structures. Numerical simulations were conducted using the ABAQUS platform to analyze the mechanical response and failure behavior of both core designs. A mesh convergence study was performed to ensure accurate and reliable simulation results. The impact tests were conducted at energy levels of 5 J, 10 J, and 20 J, while compression tests were applied with a displacement of 4 mm. The results show that the auxetic chiral core demonstrates superior performance compared to the honeycomb core by achieving smaller deformations and better energy absorption under equivalent impact forces. Furthermore, the auxetic chiral core exhibits a higher compressive strength of up to 111 MPa, outperforming the honeycomb core, which withstands only 50 MPa. Failure analysis also reveals that facesheets on auxetic panels experience significantly smaller damage areas compared to honeycomb panels. These findings indicate that auxetic chiral cores offer promising advantages for designing lightweight, impact-resistant aerospace structures.

Correspondence Author*:
Budi Aji Warsiyanto
Email:
budiaji@unsurya.ac.id

INTRODUCTION

Sandwich structures have gained significant attention in the aerospace industry due to their ability to optimize material utilization, reduce structural weight, and maintain high strength and stiffness. A typical sandwich panel consists of two thin and stiff facesheets bonded to a lightweight core, providing excellent mechanical performance under static and dynamic loading conditions [1], [2]. Among various core configurations, honeycomb cores are widely used in aircraft fuselage panels, ribs, and wing structures due to their high stiffness-to-weight ratio and energy absorption capability [3]. However, honeycomb cores also exhibit certain limitations, such as localized failure and relatively poor resistance to complex impact scenarios, including tool drops, hail damage, and bird strikes [4], [5].

Recent studies have explored auxetic chiral cores as an alternative due to their negative Poisson's ratio, which allows for enhanced energy absorption and improved damage tolerance [6], [7]. Auxetic cores expand laterally under tension, providing superior flexibility and increased resistance to delamination and localized failures compared to conventional honeycomb designs [8]. Previous works have demonstrated the potential of auxetic structures for morphing wings, impact protection, and energy absorption applications [9], [10]. Nevertheless, comparative studies between auxetic chiral and honeycomb cores under combined compression and impact loading remain limited.

Furthermore, understanding the damage mechanisms in sandwich structures under low-velocity impacts—such as tool drops or bird strikes—is critical for aerospace applications, as these events can significantly reduce the structural integrity of composite panels [11], [12]. While several numerical and experimental investigations have analyzed the impact resistance of honeycomb-based sandwich panels [13], few studies have compared them directly with auxetic chiral structures. This research addresses that gap by performing a comprehensive numerical simulation using ABAQUS to evaluate the mechanical response, energy absorption capability, and failure modes of auxetic and honeycomb sandwich panels under compression and impact loading.

METHODS

This study aims to compare the mechanical behavior of auxetic chiral and honeycomb sandwich structures under compression and low-velocity impact conditions through a finite element analysis (FEA) approach. The numerical simulations were performed using ABAQUS/Explicit, which is widely used for modeling highly nonlinear structural responses, including progressive damage and fracture in composite structures [1]. The methodology consists of geometry development, material definition, mesh convergence analysis, loading setup, and failure evaluation.

Geometrical Modeling

The sandwich panels consist of two Carbon Fiber Reinforced Polymer (CFRP) facesheets and a lightweight core made of Aluminum 2024 (Al2024), modeled using Computer-Aided Design (CAD) and imported into the Computer-Aided Engineering (CAE) platform. Two core configurations were analyzed: the auxetic chiral core, which was modeled using a dual-wave corrugated plate pattern to achieve a negative Poisson's ratio that allows lateral expansion under tension, and the honeycomb core, which was designed as a conventional hexagonal lattice for benchmarking purposes. Both panel models were designed with identical overall dimensions to ensure a consistent and accurate comparison between auxetic and honeycomb structures.

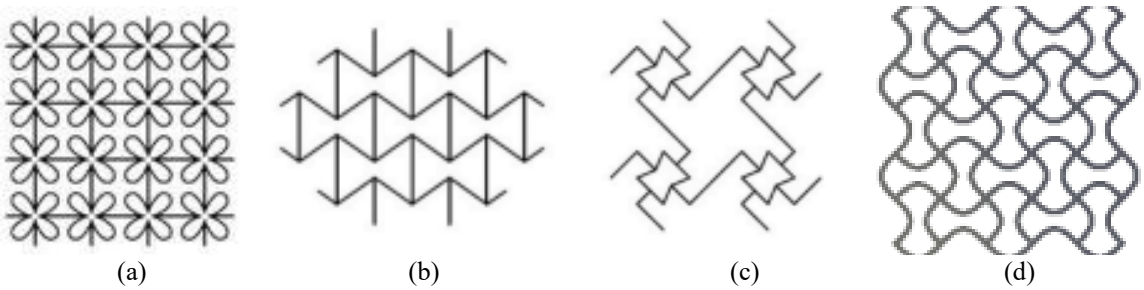

(a) (b) (c) (d)

Figure 1. Examples of 2D Auxetic Structures: (a) Semi re-entrant; (b) re-entrant honeycomb; (c) Hybrid chiral and re-entrant; and (d) Tetra-chiral 2D

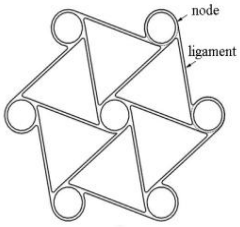

Figure 2. Nodes and Ligaments in Hexagonal Chiral Structures

Auxetic materials exhibit a negative Poisson's ratio, meaning they expand laterally when stretched, unlike conventional materials that contract [6], [7]. Several forms of auxetic structures exist, including semi re-entrant, re-entrant honeycomb, hybrid chiral re-entrant, and tetra-chiral configurations, as illustrated in Figure 1 [8], [9]. In the chiral auxetic structure, nodes and ligaments play a crucial role in determining the overall mechanical behavior and deformation response. As illustrated in Figure 2, ligaments act as connecting elements between nodes and are responsible for maintaining structural integrity, stiffness, and flexibility [10], [11]. The geometric configuration and ligament properties directly affect the lattice stiffness and auxetic response. The auxetic chiral design enables deterministic cell rotations, where the individual cells rotate in a specific direction during deformation, resulting in enhanced energy absorption and improved resistance to local damage [12]–[14].

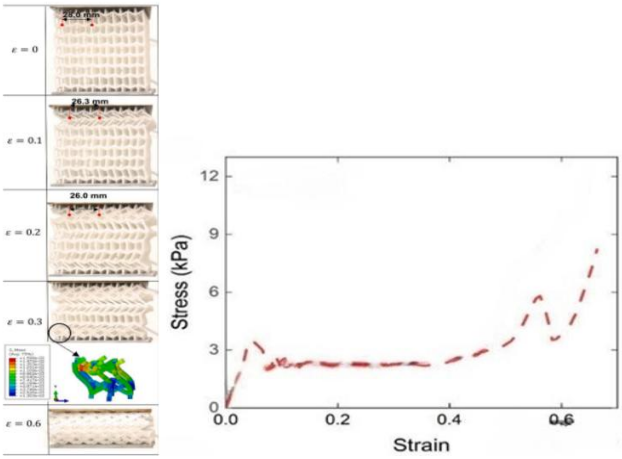

Figure 3. Stress–Strain Curve of Auxetic Core

Additionally, the mechanical response of auxetic materials was evaluated using stress–strain curves shown in Figure 3 [16]. Initially, the auxetic core maintains its structural integrity without noticeable deformation. As stress increases and approaches the elastic limit, the material returns to its original shape when unloaded. However, beyond this limit, plastic deformation occurs, leading to permanent structural changes. At a strain of approximately 0.1, the first layer of upper cells begins to fail, followed by progressive cell collapse in subsequent layers, which causes a sharp increase in stress until the auxetic core experiences significant damage accumulation. This comprehensive geometrical modeling approach provides a more accurate understanding of the structural behavior of auxetic and honeycomb cores under compression and impact loading, allowing a more reliable comparison between both configurations.

Material Properties

The material properties for Al2024 cores and CFRP facesheets were defined based on experimental data and relevant literature [18], [13]. Table 1 summarizes the key parameters applied in the simulation.

Tabel 1 Property material Al2024[18]

Parameters	Material Parameters
Elastic modulus	$73000Mpa$
Poisson's ratio	0.3
Density	$2780kg/m^3$

Tabel 2 Property material CFRP[13]

Parameters	Material Parameters
Elastic modulus	$E_1 = 120.000Mpa, E_2 = E_3 = 7800Mpa$
Poisson's ratio	$v_{12} = v_{13} = v_{23} = 0.3$
Shear modulus	$G_{12} = G_{13} = 4000Mpa, G_{23} = 3600Mpa$
Density	$\rho = 2000kg/m^3$
Ultimate strength	$X^T = 1800Mpa, X^c = 1250Mpa, Y^T = Z^T = 50Mpa, Y^C = Z^C = 150Mpa,$ $S_{12} = S_{13} = 93Mpa, S_{23} = 50Mpa$
Fracture energy	$G_{11}^T = G_{11}^C = 40kJ/m^2, G_{22}^T = 0.25kJ/m^2, G_{22}^C = 0.75kJ/m^2$

Simulation Setup and Failure Analysis

The numerical simulations were conducted using ABAQUS/Explicit, following a structured setup process to ensure accurate and reliable results. The simulation procedure consisted of several key stages, including geometry modeling, material property definition, assembly creation, step assignment, boundary conditions, loading configurations, mesh refinement, and job submission. The overall workflow of the numerical modeling process is illustrated in Figure 4.

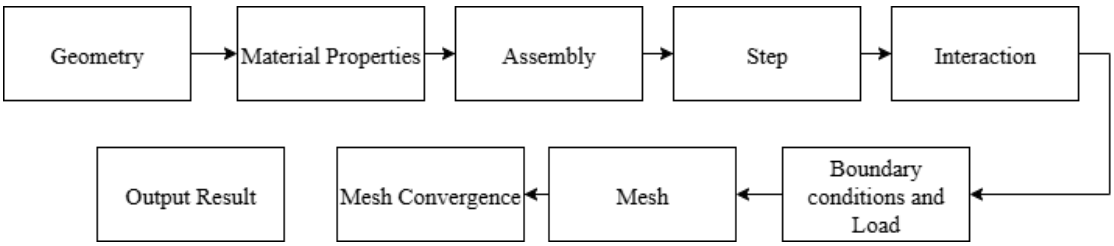

Figure 4. Numerical Simulation Setup Workflow

The simulations involved two types of loading conditions: low-velocity impact tests and compression tests. For the impact simulations, a rigid impactor with a mass of 1.15 kg was applied at energy levels of 5 J, 10 J, and 20 J to replicate realistic scenarios such as tool drops and bird strikes. For the compression simulations, a displacement-controlled loading of 4 mm was applied to the top facesheet, while the edges of the sandwich panel were fully fixed to evaluate its compressive strength and overall structural stability.

To ensure solution accuracy and computational efficiency, a mesh convergence study was performed. Three different mesh densities were tested to determine the optimal configuration. The final mesh size was selected based on convergence criteria, ensuring that the variation in maximum stress remained within 5% across different refinement levels. This approach ensured that the simulation results were both accurate and reliable.

For damage and failure prediction, the Hashin failure criteria [5] were implemented to evaluate multiple composite failure modes, including fiber tension (FT), fiber compression (FC), matrix tension (MT), and matrix compression (MC). The evolution of damage variables was tracked throughout the simulations to analyze localized failure patterns, potential delamination behavior, and the residual strength of both auxetic and honeycomb sandwich panels under different loading scenarios.

Fibre Tension, FT ($\sigma 11 \geq 0$):

$$\left(\frac{\sigma_{11}}{X^T}\right)^2 + \left(\frac{T_{12}}{S^L}\right)^2 = 1 \quad (1)$$

Fiber Compression, FC ($\sigma 11 < 0$):

$$\left(\frac{\sigma_{11}}{X^C}\right)^2 = 1 \quad (2)$$

Matrix Tension, MT ($\sigma 22 \geq 0$):

$$\left(\frac{\sigma_{22}}{Y^T}\right)^2 + \left(\frac{\tau_{12}}{S^L}\right)^2 = 1 \tag{3}$$

Matrix Compression, MC ($\sigma 22 < 0$):

$$\left(\frac{\sigma_{22}}{2S^T}\right)^2 + \left[\left(\frac{Y^C}{2S^T}\right)^2 - 1\right]\frac{\sigma_{22}}{Y^C} + \left(\frac{\tau_{12}}{S^L}\right)^2 = 1 \tag{4}$$

RESULT AND DISCUSSION

This section presents the numerical simulation results and analysis of the structural performance of the auxetic chiral and honeycomb sandwich panels under impact and compression loading. The results are divided into four subsections: impact test analysis, deformation mechanism, compression test analysis, and facesheet damage evaluation.

Impact Test Analysis

Numerical simulations were conducted to investigate the low-velocity impact behavior of the sandwich panels at energy levels of 5 J, 10 J, and 20 J. A rigid impactor with a mass of 1.15 kg was used to replicate realistic scenarios commonly encountered in aerospace applications, such as tool drops, hail impacts, and runway debris.

Figure 5 presents the comparison of contact force–displacement curves for auxetic and honeycomb cores under different impact energies. The auxetic core consistently demonstrates higher peak forces and better energy absorption compared to the honeycomb core. At 5 J, the auxetic core withstands a maximum force of 9.18 kN with an upper facesheet deformation of approximately 1.14 mm, outperforming the honeycomb core, which reaches 5.81 kN with 1.06 mm deformation. At 10 J, the auxetic panel achieves 11.53 kN and 1.53 mm deformation, compared to the honeycomb core at 7.71 kN and 1.66 mm. Finally, at 20 J, the auxetic core sustains 16.99 kN with 2.15 mm deformation, whereas the honeycomb panel resists 13.21 kN but undergoes 2.54 mm deformation.

The area enclosed by the curves in Figure 5 represents the energy dissipated during the impact. It can be observed that the auxetic core absorbs more energy while maintaining smaller deformation, indicating its higher damage tolerance. Additionally, as the impact energy increases, the overall damage and maximum deflection of the sandwich structures also increase significantly, which aligns with the progressive failure observed in high-energy impact events.

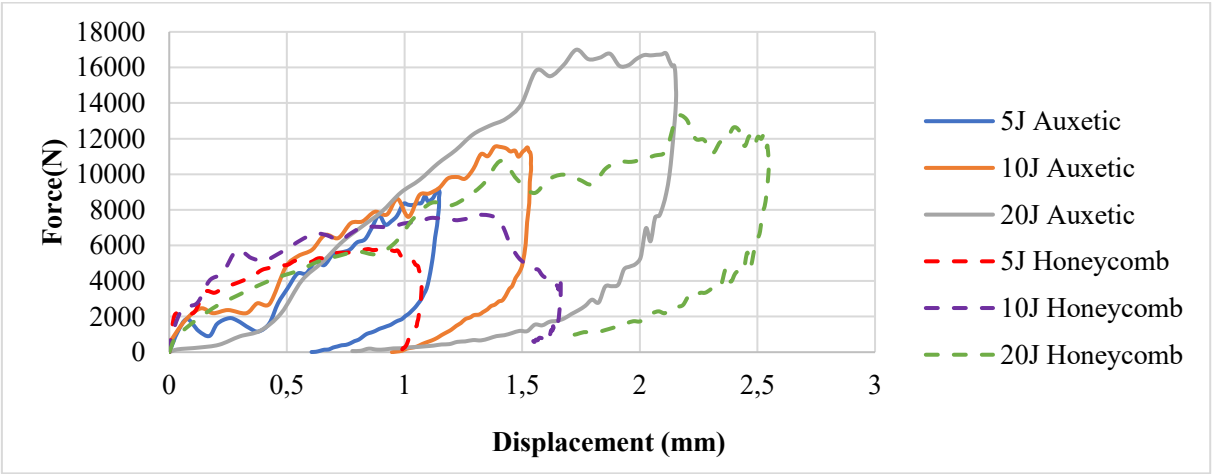

Figure 5. Comparison of force–displacement curves for auxetic and honeycomb cores under different impact energies

Deformation Mechanism Under Impact

The deformation mechanisms of the auxetic chiral and honeycomb cores under low-velocity impact are illustrated in Figures 6 and 7. At 5 J, both the auxetic chiral and honeycomb cores exhibit no significant cell wall deformation, maintaining structural integrity. At 10 J, the auxetic chiral core continues to remain stable with minimal deformation, whereas the honeycomb core starts showing initial buckling in several cells. At 20 J, the auxetic chiral core begins to experience localized cell wall fractures, while the honeycomb core undergoes severe buckling and widespread cell collapse, leading to reduced energy absorption capacity.

These findings highlight the superior damage resistance of the auxetic chiral core, which delays structural failure compared to the conventional honeycomb design. The unique auxetic behavior, resulting from the negative Poisson's ratio, enables better stress redistribution, allowing the auxetic core to maintain integrity under higher energy impacts.

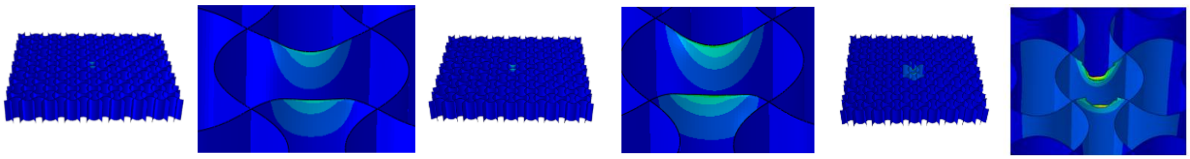

(a) (b) (c)

Figure 6. Deformation of auxetic core at impact energies of (a) 5J; (b) 10J, (c) and 20J

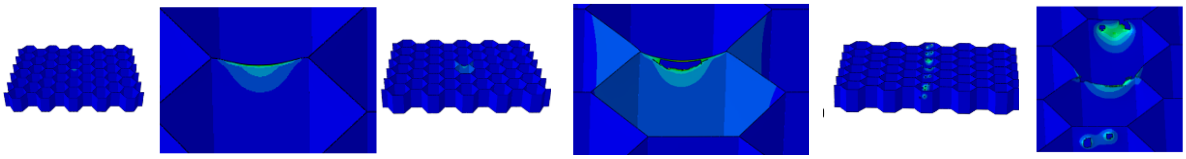

(a) (b) (c)

Figure 7. Deformation of honeycomb core at impact energies of (a) 5J; (b) 10J, (c) and 20J

Compression Test Analysis

Compression simulations were performed using a 4 mm displacement-controlled loading applied to the top facesheet of the sandwich panel, while the edges were fully constrained. The displacement of 4 mm represents the threshold where the structures begin to experience significant deformation and loss of initial stiffness.

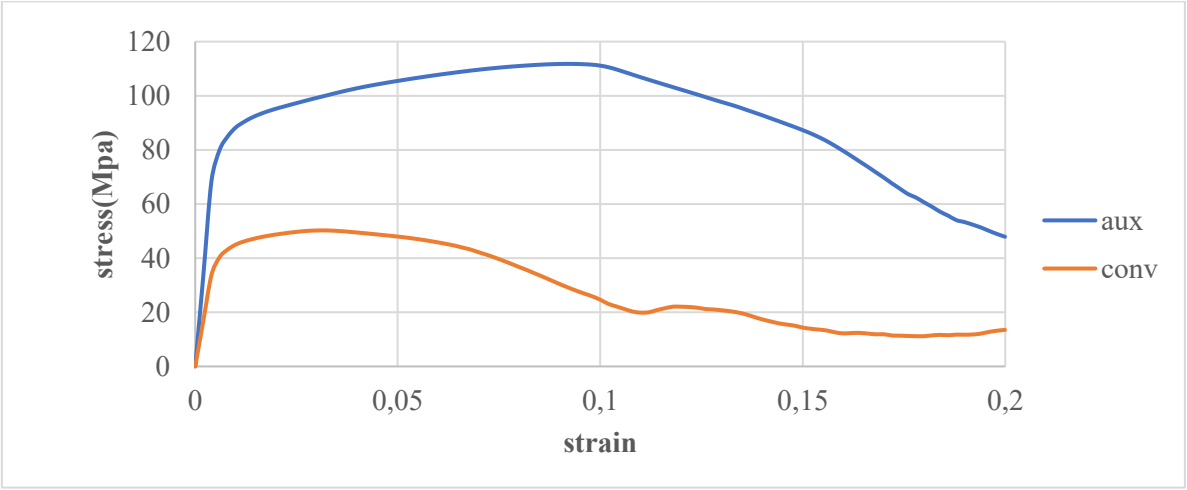

Figure 8. Stress–strain curves of auxetic and honeycomb cores under compression

The stress–strain responses of both cores are shown in Figure 8. The auxetic core achieves a maximum compressive strength of approximately 111 MPa, whereas the honeycomb core sustains only 50 MPa. During the elastic stage, both cores maintain their geometry, but once the stress exceeds the elastic limit, the honeycomb core experiences early cell wall buckling, resulting in a non-linear stress–strain response. As loading progresses, the honeycomb core undergoes progressive collapse and cell wall folding, leading to a significant reduction in its load-carrying capacity. In contrast, the auxetic core demonstrates higher resistance to failure due to its unique chiral rotation mechanism, which delays the onset of instability.

The deformation sequence for both cores under compression is illustrated in Figure 9. At 0.25 s, both cores begin to exhibit initial deformation. At 0.5 s, the auxetic core starts to experience controlled buckling, whereas the honeycomb core shows severe folding and begins to lose stability rapidly. By 1.0 s, the honeycomb structure collapses almost entirely, while the auxetic core maintains better structural integrity.

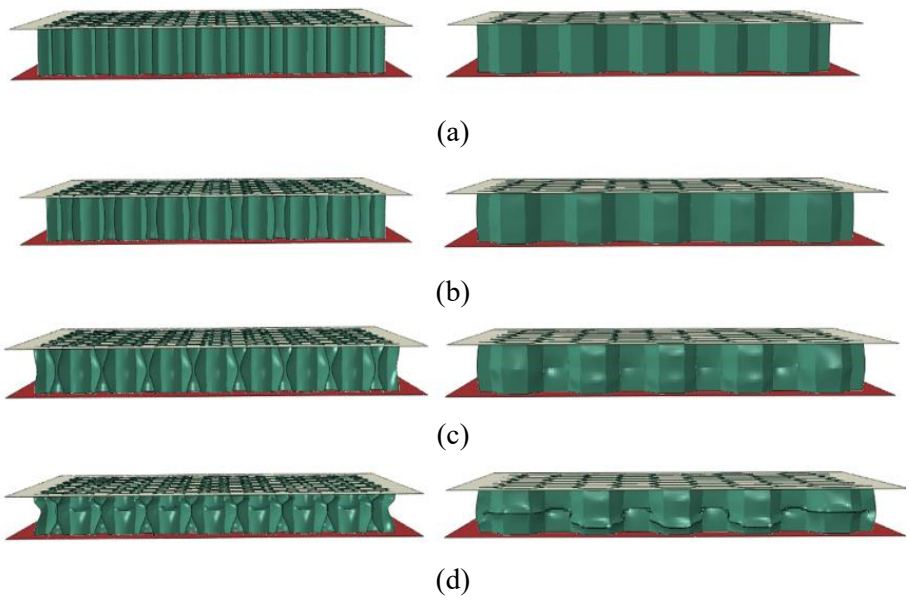

Figure 9. Compression deformation sequence of auxetic and honeycomb cores at (a) 0s; (b) 0.25s, (c) 0.5s; and (d) 1s

Facesheet Damage Evaluation

The damage evaluation of the facesheets was conducted using the Hashin failure criteria, which classify composite damage into four failure modes: matrix compression and shear (MC), matrix tension (MT), fiber tension (FT), and fiber compression (FC). In the Abaqus simulations, the failure of the facesheet is indicated numerically, where a value of 1 represents the point at which the material is considered to have failed (HSNFCCRT index).

The simulations were performed using a 1.15 kg impactor at energy levels of 5 J, 10 J, and 20 J for both auxetic and honeycomb cores. In all scenarios, the facesheets experienced varying levels of damage, including fiber tearing and matrix cracking. Figures 10 to 12 illustrate the facesheet damage for the auxetic core under impact energies of 5 J, 10 J, and 20 J, respectively. At lower energies, minimal matrix cracking and fiber damage are observed, whereas at 20 J, localized delamination begins but remains confined to smaller regions due to better energy dissipation.

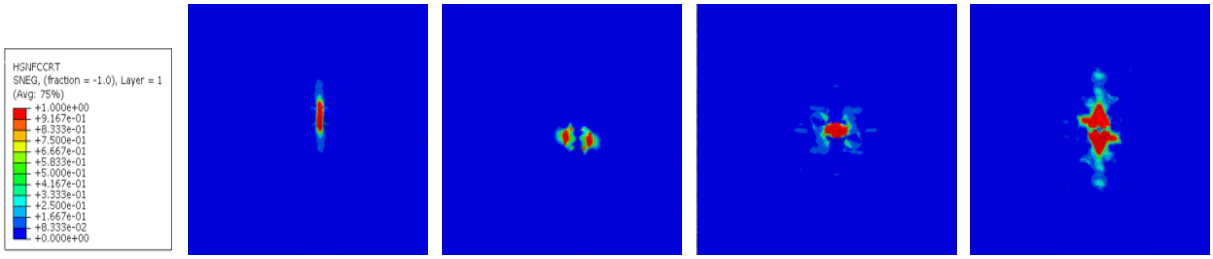

(a) (b) (c) (d)

Figure 10. Damage distribution on the auxetic core facesheet under 5 J impact energy: (a) fiber compression (FC), (b) fiber tension (FT), (c) matrix compression (MC), and (d) matrix tension (MT).

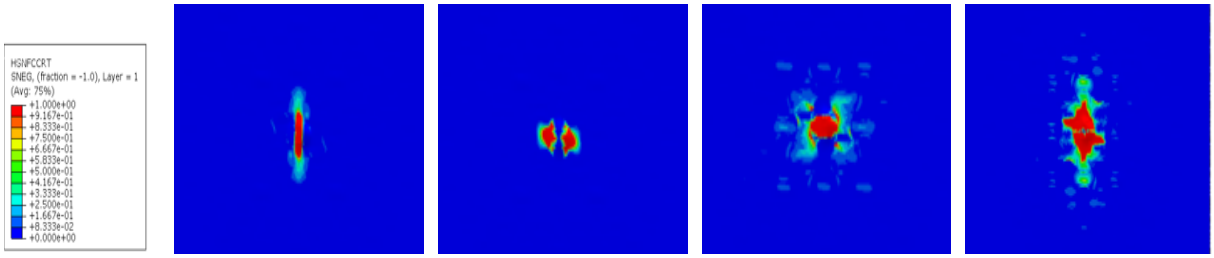

(a) (b) (c) (d)

Figure 11. Damage distribution on the auxetic core facesheet under 10 J impact energy: (a) fiber compression (FC), (b) fiber tension (FT), (c) matrix compression (MC), and (d) matrix tension (MT)

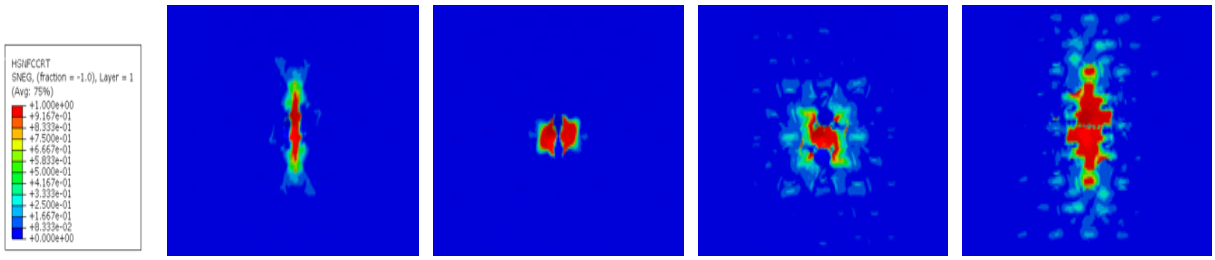

(a) (b) (c) (d)

Figure 12. Damage distribution on the auxetic core facesheet under 20 J impact energy: (a) fiber compression (FC), (b) fiber tension (FT), (c) matrix compression (MC), and (d) matrix tension (MT).

In contrast, Figures 13 to 15 show the facesheet damage for the honeycomb core under the same impact energies. Unlike the auxetic design, the honeycomb facesheets exhibit wider damage zones and extensive matrix cracking at 10 J and 20 J, indicating lower structural resilience.

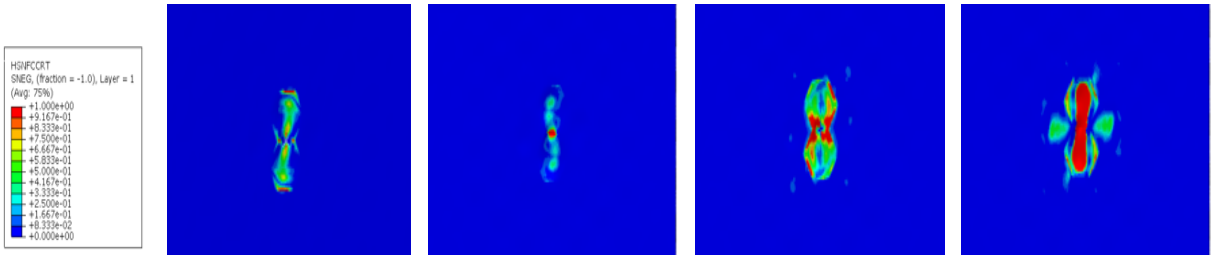

(a) (b) (c) (d)

Figure 13. Damage distribution on the honeycomb core facesheet under 5 J impact energy: (a) fiber compression (FC), (b) fiber tension (FT), (c) matrix compression (MC), and (d) matrix tension (MT).

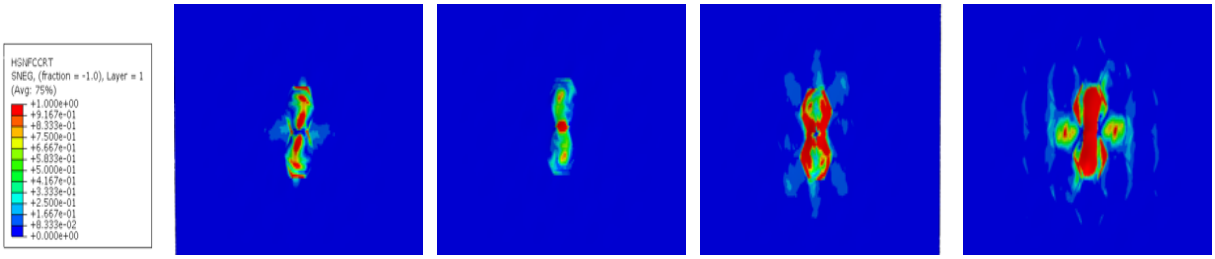

(a) (b) (c) (d)

Figure 14. Damage distribution on the honeycomb core facesheet under10 J impact energy: (a) fiber compression (FC), (b) fiber tension (FT), (c) matrix compression (MC), and (d) matrix tension (MT).

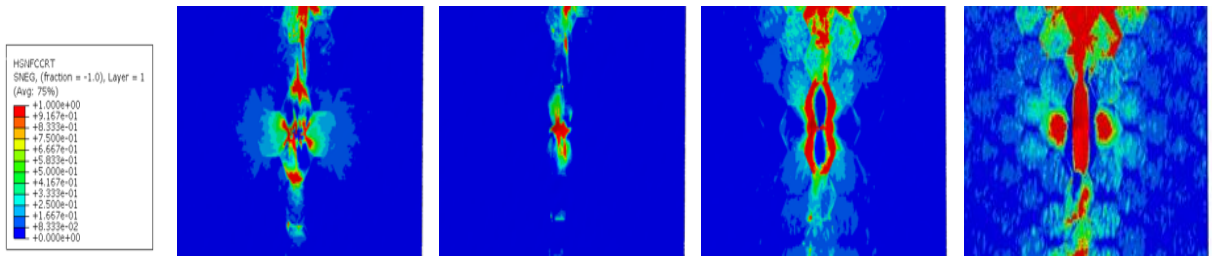

(a) (b) (c) (d)

Figure 15. Damage distribution on the honeycomb core facesheet under 20 J impact energy: (a) fiber compression (FC), (b) fiber tension (FT), (c) matrix compression (MC), and (d) matrix tension (MT).

As shown in Figures 10–15, the damaged area expands significantly with increasing impact energy. At lower energies (5 J), the facesheet damage is relatively localized, whereas at higher energies (20 J), the damage spreads widely across the impacted region.

Comparisons between auxetic and honeycomb cores reveal distinct differences in damage tolerance. In the auxetic core, damage zones remain relatively confined due to the negative Poisson's ratio, which redistributes impact stresses more efficiently. In contrast, the honeycomb core exhibits larger and more severe damage regions, showing lower overall resistance to high-energy impacts.

CONCLUSIONS

This study presents a comparative numerical analysis of auxetic chiral and honeycomb sandwich panels under low-velocity impact and compression loading using ABAQUS/Explicit. The results show that auxetic cores consistently achieve higher peak forces, smaller deformations, and greater energy absorption under impact energies of 5 J, 10 J, and 20 J. In compression tests, the auxetic panels sustain a maximum stress of 111 MPa, more than double that of honeycomb panels (50 MPa), while delaying buckling initiation due to their chiral cell rotation mechanism.

Facesheet damage evaluation confirms that auxetic panels exhibit smaller localized damage zones, whereas honeycomb structures experience wider matrix cracking and fiber rupture at similar energy levels. From a practical perspective, auxetic cores are more suitable for aircraft structures exposed to medium to high dynamic impact risks, such as fuselage panels, wing ribs, and protective components.

Overall, this research contributes to the development of advanced sandwich structures in aerospace engineering by demonstrating the superior impact resistance, damage tolerance, and structural integrity of auxetic designs, providing a strong foundation for future applications in next-generation aircraft.

ACKNOWLEDGMENTS

The authors would like to express their sincere gratitude to the Aeronautical Engineering Study Program, Faculty of Aerospace and Industrial Engineering, and Universitas Dirgantara Marsekal Suryadarma (Unsurya) for providing academic and technical support throughout this research. Special thanks are also extended to the Structural Mechanics and Numerical Simulation Laboratory for granting access to the computational resources required to conduct the finite element simulations in ABAQUS/Explicit.

This research would not have been possible without the valuable discussions, constructive feedback, and encouragement from colleagues and collaborators involved in the project. The authors also acknowledge the facilities and environment provided by the university, which have significantly contributed to the successful completion of this work.

REFERENCES

[1] K. J. Al-Fatlawi, K. Jármai, and G. Kovács, "Optimization of a totally fiber-reinforced plastic composite sandwich construction of helicopter floor for weight saving, fuel saving and higher safety," *Polymers*, vol. 13, no. 16, pp. 1–16, 2021.
[2] S. N. Abhinav, "A review paper on origin of honeycomb structure and its sailing properties," *Int. J. Eng. Res.*, vol. 9, no. 8, pp. 861–866, 2020.
[3] C. İnan, Z. Evis, and B. Ozturk, "Structural comparison of conventional and chiral auxetic morphed aircraft rib," *Mater. Test.*, vol. 66, 2023.
[4] M. Altay, "A review of auxetic structures with chiral cores for morphing wing applications," 2018.
[5] Y. Zhang et al., "In-plane compressive properties of assembled auxetic chiral honeycomb composed of slotted wave plate," *Mater. Des.*, vol. 221, p. 110956, 2022.
[6] I. A. Shah et al., "Finite element analysis of the ballistic impact on auxetic sandwich composite human body armor," *Materials*, vol. 15, no. 6, pp. 1–16, 2022.
[7] S. Dong and H. Hu, "Sensors based on auxetic materials and structures: A review," *Materials*, vol. 16, no. 9, pp. 1–20, 2023.
[8] A. Mauko et al., "Dynamic deformation behaviour of chiral auxetic lattices at low and high strain-rates," *Metals*, vol. 11, no. 1, pp. 1–15, 2021.
[9] K. Gunaydin, H. S. Türkmen, A. Airoldi, M. Grasso, G. Sala, and A. M. Grande, "Compression behavior of EBM printed auxetic chiral structures," *Materials*, vol. 15, no. 4, pp. 1–21, 2022.
[10] R. Gatt et al., "On the effect of the mode of connection between the node and the ligaments in anti-tetrachiral systems," *Adv. Eng. Mater.*, vol. 17, pp. 1–12, 2014.
[11] E. Montgomery-Liljeroth, S. Schievano, and G. Burriesci, "Elastic properties of 2D auxetic honeycomb structures: A review," *Appl. Mater. Today*, vol. 30, p. 101722, 2023.
[12] Q. Hu, G. Lu, and K. M. Tse, "Compressive and tensile behaviours of 3D hybrid auxetic-honeycomb lattice structures," *Int. J. Mech. Sci.*, vol. 263, p. 108767, 2024.
[13] H. Hu et al., "Progressive damage behaviour analysis and comparison with 2D/3D Hashin failure models on carbon fibre–reinforced aluminium laminates," *Polymers*, vol. 14, p. 2946, 2022.
[14] J. X. Wang, Q. S. Yang, Y. L. Wei, and R. Tao, "A novel chiral metamaterial with multistability and programmable stiffness," *Smart Mater. Struct.*, vol. 30, no. 6, 2021.
[15] Y. Jiang and Y. Li, "3D printed auxetic mechanical metamaterial with chiral cells and re-entrant cores," *Sci. Rep.*, vol. 8, pp. 1–11, 2018.
[16] H. Huang, B. Wong, and Y. Chou, "Design and properties of 3D-printed chiral auxetic metamaterials by reconfigurable connections," *Phys. Status Solidi*, vol. 253, pp. 1–8, 2016.
[17] Z. Hashin, "Failure criteria for unidirectional fiber composites," *J. Appl. Mech.*, vol. 47, no. 2, pp. 329–334, 1980.
[18] ASM International, "ASM Material Data Sheet: Aluminum 2024-T3," Accessed: Aug. 25, 2024. [Online]. Available: https://asm.matweb.com